

**Study on Worm Defect in 6061 Aluminum Alloy Friction Stir Welded Plates**

by

**Ahmad Khalil Bin Ahmad Radzi**

Dissertation submitted in the partial fulfilment of  
the requirement for the  
Bachelor of Engineering (Hons)  
(Mechanical Engineering)

MAY 2011

**Universiti Teknologi PETRONAS**

**Bandar Seri Iskandar**

**31750 Tronoh**

**Perak Darul Ridzuan**

**CERTIFICATION OF APPROVAL**

**Study on Worm Defect in 6061 Aluminum Alloy Friction Stir Welded Plates**

**by**

**Ahmad Khalil Bin Ahmad Radzi**

**A project dissertation submitted to the  
Mechanical Engineering Programme  
Universiti Teknologi PETRONAS  
in partial fulfilment of the requirement for the  
Bachelor of Engineering (Hons)  
(Mechanical Engineering)**

Approved by,



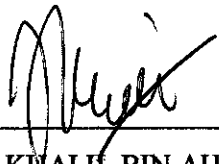
---

(Dr. Mokhtar Awang)

**UNIVERSITI TEKNOLOGI PETRONAS  
TRONOH, PERAK  
MAY 2011**

## CERTIFICATION OF ORIGINALITY

This is to certify that I am responsible for the work submitted in this project, that the original work is my own except as specified in the references and acknowledgements, and that the original work contained herein have not been undertaken or done by unspecified sources or persons.



---

AHMAD KHALIL BIN AHMAD RADZI

## ABSTRACT

Friction stir welding (FSW) is a solid-state joining process where the original characteristics of metal remain unchanged. The technique results in high joint strength compared with other welding techniques. It has been widely used for joining aluminum alloys in the fields of aerospace, marine, automotive, rail and many other applications of commercial importance [1]. Some important process parameters that should be taken into account and control the quality of the weld are the tool spindle speed (rpm), transverse speed (mm/min), plunging speed (mm/min), dwell time (s) and depth of penetration (mm). Studies have shown that during FSW, wormhole (tunnel) defect form along the welded area and the evolved microstructure strongly affects the mechanical properties of the joint. In this investigation, an attempt has been made to understand the influence of welding parameters on worm defect in 6061 aluminum alloy plates. For this project, nine (9) different set of welding parameter combination were used to fabricate the FSW joints. The scope of study is to butt joined two (2) pieces of 6061 aluminum alloy plates having the dimension of 100mm x 100mm x 10mm and by rigidly clamped both pieces to perform the welding operation. The project will focus on tapered pin tool design using AISI H13 Tool Steel Grade. The welding tool will be fabricated using BridgePort PowerPath 15 (CNC Lathe Machine) and undergo heat treatment to increase the hardness level. Meanwhile, the welding process will be conducted using BridgePort VMC 2216 (CNC Milling Machine). By using Optical Microscope (OM), the size worm defect is measured. Microhardness measurements were taken on cross sections of the specimen and were correlated with the size of wormhole defect. The result concludes that increase in ratio of tool transverse feed rate (S) to tool spindle speed (N) will result in increase in the wormhole size (mm<sup>2</sup>) and decrease in Vickers Microhardness (HV) value.

## **ACKNOWLEDGEMENT**

First and foremost, the author would like to express his utmost gratitude and appreciation to Allah for giving the author His blessings and help, the Final Year Project went smoothly. Alhamdulillah, all praises to Him that the author has been able to complete this project in the time given.

The project would not have been possible without the assistance and guidance of certain individuals whose contributions have helped in its completion. The author would like to express his sincere thanks and appreciation to the Project Supervisor, Dr. Mokhtar Awang for giving his trust and provide the author with ample support and guidance throughout the whole period of completing the final year project. All of his effort and assistance from the beginning to the end of this study really help the author in the project completion.

Special express gratitude is also reserved for the Mechanical Engineering Department of Universiti Teknologi PETRONAS for providing excellent support in terms of providing cutting edge knowledge and information not just within the Final Year Project but also the five (5) years spent undergoing every single bit of invaluable knowledge on Mechanical Engineering as a whole. The author would also like to deliver his warmth appreciation to the technical staffs who are involved with this project, namely Mr. Shaiful Hisham, Mr. Jani Alang Ahmad, Mr. Mahfuz, Mr. Paris and also Mechanical Engineering Postgraduate (PG) student Mr. Umar Patthi for assisting with the technical support and guidance towards this project.

Finally, thanks to family members of the author and fellow colleagues for their valuable assistance throughout the completion of this study. I hope that the outcome of this report will bring beneficial output to others as well. Thank you very much everyone.

## TABLE OF CONTENTS

<b>CERTIFICATION OF APPROVAL</b>	.	.	.	.	.	.	.	<b>i</b>
<b>CERTIFICATION OF ORIGINALITY</b>	.	.	.	.	.	.	.	<b>ii</b>
<b>ABSTRACT</b>	.	.	.	.	.	.	.	<b>iii</b>
<b>ACKNOWLEDGEMENT</b>	.	.	.	.	.	.	.	<b>iv</b>
<b>TABLE OF CONTENT</b>	.	.	.	.	.	.	.	<b>v</b>
<b>LIST OF FIGURES</b>	.	.	.	.	.	.	.	<b>vii</b>
<b>LIST OF TABLES</b>	.	.	.	.	.	.	.	<b>ix</b>
<b>CHAPTER 1:</b>								
<b>INTRODUCTION</b>	.	.	.	.	.	.	.	<b>1</b>
1.1	Project Background	.	.	.	.	.	.	<b>1</b>
1.2	Problem Statement	.	.	.	.	.	.	<b>5</b>
1.3	Objective	.	.	.	.	.	.	<b>5</b>
1.4	Scope of Study.	.	.	.	.	.	.	<b>5</b>
<b>CHAPTER 2:</b>								
<b>LITERATURE REVIEW</b>	.	.	.	.	.	.	.	<b>7</b>
<b>CHAPTER 3:</b>								
<b>METHODOLOGY</b>	.	.	.	.	.	.	.	<b>12</b>
3.1	Research on AISI Tool Steel H13	.	.	.	.	.	.	<b>12</b>
3.2	Fabrication of Welding Tool	.	.	.	.	.	.	<b>14</b>
3.3	Work piece Preparation.	.	.	.	.	.	.	<b>15</b>
3.4	Heat Treatment of H13 AISI Tool Steel	.	.	.	.	.	.	<b>15</b>

3.5	Hardness of Tool Steel	.	.	16
3.6	Friction Stir Welding Process.	.	.	18
3.7	Sample Preparation	.	.	19
3.7.1	Sectioning	.	.	20
3.7.2	Mounting	.	.	21
3.7.3	Grinding and Polishing	.	.	22
3.7.4	Etching	.	.	23
3.8	Wormhole Size Measurement.	.	.	23
3.9	Vicker Microhardness Testing	.	.	24
3.10	Key Milestones	.	.	26
3.11	Project Work Flow (FYP II)	.	.	27
<b>CHAPTER 4:</b>	<b>RESULTS AND DISCUSSION</b>	.	.	<b>28</b>
4.1	Welding Parameters	.	.	28
4.2	Welding Results	.	.	29
4.3	Material Characterization	.	.	31
4.4	Wormhole Size Analysis.	.	.	33
4.5	Microhardness Testing	.	.	37
4.6	Heat Generation in FSW	.	.	39
<b>CHAPTER 5:</b>	<b>CONCLUSION AND RECOMMENDATIONS</b>	.	.	<b>43</b>
5.1	Conclusions	.	.	43
5.2	Recommendations	.	.	44
<b>REFERENCES</b>	.	.	.	<b>44</b>
<b>APPENDICES</b>	.	.	.	<b>47</b>

## LIST OF FIGURES

Figure 1.1	Schematic of Friction Stir Welding (FSW)	2
Figure 1.2	FSW Run That Was Done Using Bridgeport 2216 (CNC Milling Machine).	2
Figure 1.3	Various Microstructural Regions in the Traverse Cross Section of A Friction Stir Welding (FSW) Material	3
Figure 1.4	Friction Stir Welding (FSW) Weld between Aluminum Sheets & wormhole formation indicated in Aluminium Alloy plate.	4
Figure 2.1	Evolution of a Defect-Free Weld as a Function of the Shoulder Interaction with the Base Material.	11
Figure 3.1	Design of Cylindrical Tapered Pin H13 Tool Steel using AutoCAD 2007	14
Figure 3.2	Temperature Profile during the Heat Treatment Process	16
Figure 3.3	Carbolite Tube Furnace.	16
Figure 3.4	OMAG Brevetti Affri Hardness Testers	17
Figure 3.5	The Raw H13 Tool Steel (Left) and Finish Product after Heat Treatment (Right)	18
Figure 3.6	FSW Run is completed using BridgePort VMC 2216 (CNC Milling Machine)	19
Figure 3.7	Sectioning of Aluminium Alloy Plates using KP-280 Linear Hacksaw Machine	20
Figure 3.8	Delta Non-Ferrous Abrasive Cutter	21
Figure 3.9	BUEHLER Auto Mounting Press Machine	22
Figure 3.10	BUEHLER Special Silicon Carbide Grinding Paper	22
Figure 3.11	Grinding Process of Mounted Aluminium Alloy Sample with Water as Lubricant	23

Figure 3.12	Leica DMLM Optical Microscope . . . . .	24
Figure 3.13	Schematic Illustrating the Local Increase in Particle Concentration Due To Indentation . . . . .	25
Figure 3.14	The Vicker Microhardness (HV) of Prepared FSW Sample is taken using LECO LM247 AT Microhardness Testing Machine . . . . .	25
Figure 3.15	Project Work Flow (FYP II). . . . .	27
Figure 4.1	Weld Path with Respective Labeling . . . . .	29
Figure 4.2	Wormhole Defect Appears at the Grinded Sample . . . . .	30
Figure 4.3	Graphical Result of Elemental Analysis using FESEM Displayed on the Monitor . . . . .	32
Figure 4.4	SmartSEM EDS INCA Energy Machine . . . . .	33
Figure 4.5	Wormhole Images Taken using Non-Contact Measurement . . . . .	33
Figure 4.6	Measurement of Wormhole Size using Optical Microscope . Machine . . . . .	34
Figure 4.7	Histogram Showing Each FSW Run with the Corresponding Size of Wormhole Cross Sectioned Area (mm <sup>2</sup> ) . . . . .	36
Figure 4.8	Graph Microhardness (HV) vs. Distance from Weld Center (mm)	38
Figure 4.9	Graph Microhardness (HV) vs. Wormhole Size (mm <sup>2</sup> ) . . . . .	39
Figure 4.10	Wormhole Size (mm <sup>2</sup> ) vs. Welding Parameter Ratio S: N . . . . .	41
Figure 4.11	Graph Microhardness (HV) vs. Welding Parameter Ratio S: N	42

## LIST OF TABLES

Table 2.1	Selection of Tool Design at the Welding Institute (TWI)	9
Table 3.1	Chemical Composition of AISI H13 Tool Steel	13
Table 3.2	Hardness of Welding Tool Steel H13 Before and After Heat Treatment Process.	17
Table 4.1	Constant spindle speed (N) of 1,100 rpm	28
Table 4.2	Constant spindle speed (N) of 2,200 rpm	28
Table 4.3	Constant feed rate (S) of 50 mm/min	29
Table 4.4	Sectioned Wormhole Region	29
Table 4.5	Elemental Analysis of the Aluminum Alloy Sample	31
Table 4.6	Results of Measured Average Wormhole Area (mm <sup>2</sup> )	35
Table 4.7	Result of Microhardness Testing.	37
Table 4.8	Result of Heat Generated Calculation	41
Table 4.9	Relationship of Ratio (S: N), Heat Generated (Q), Wormhole Size (mm <sup>2</sup> ) and Microhardness	41

# CHAPTER 1

## INTRODUCTION

### 1.1 Project Background

Welding is defined as a joining process that produces coalescence of materials by heating them to the welding temperature, with or without the application of pressure or by the application alone, and with or without the use of filler metal. A weld joint is done when separate pieces of metal is to be join and becoming one piece when heated to a temperature high enough to cause softening or melting and flow together [2]. Here, **Friction Stir Welding (FSW)** can be taken as an example and also the intended welding process for this project.

Friction Stir Welding (FSW) was invented at The Welding Institute (TWI) of the United Kingdom in 1991 which uses heat generated by friction (rubbing) to fuse two pieces of metal together and was initially applied to aluminum alloys. The friction stir process involves the translation of a rotating cylindrical tool (non-consumable tool) along the interface between two plates. Friction heats the material which is then essentially extruded around the tool before being forged by the large down pressure. The simultaneous rotational and translational motion of the welding tool during the welding process creates a characteristic asymmetry between the adjoining sides. On one side, where the tool rotation is with the direction of the translation of the welding tool is called the advancing side (AS), whereas on the other side, the two motions, rotation and translation counteract is called the retreating side (RS). The welding process does not require special preparation of the sample and little waste or pollution is created during the welding process. Furthermore, its applicability to aluminum alloys, in particular dissimilar alloys or those considered “unweldable” by conventional welding techniques, such as Tungsten Inert Gas (TIG) welding, makes it as an attractive method for the transportation sector [3].



Generally, Friction Stir Welding (FSW) joints consist of four (4) different regions which are illustrated in Figure 1.3. The four regions are [5]:

**A. Unaffected Material or Parent Metal**

It is the material remote from the weld that has not been deformed. Although it may have experienced a thermal cycle from the weld, it is not affected by the heat in terms of microstructure or mechanical properties.

**B. Heat Affected Zone (HAZ)**

Here (closer to the weld center), the material has experienced a thermal cycle that has modified the microstructure and the mechanical properties. However, there is no plastic deformation occurring in this area.

**C. Thermomechanically Affected Zone (TMAZ)**

In this region, the FSW tool has plastically deformed the material. The heat from the process will also have exerted some influence on the material. For aluminum, it is possible to obtain significant plastic strain without recrystallization in the region, and there is generally a distinct boundary between recrystallized zone (weld nugget) and the deformed zones of TMAZ.

**D. Weld Nugget:**

The fully recrystallized area sometimes called the stir zone, refers to the zone previously occupied by the tool pin. The term stir zone is commonly used in friction stir processing, where large volumes of material are processed.

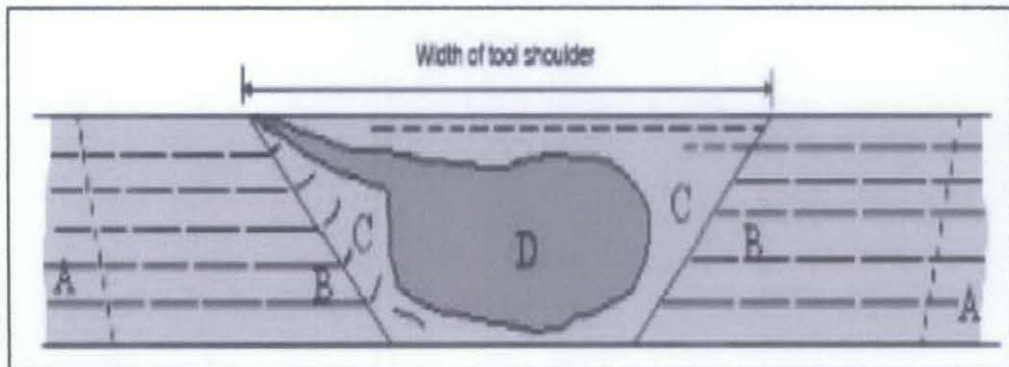


**Figure 1.3: Various Microstructural Regions in the Traverse Cross Section of a Friction Stir Welding (FSW) Material [5]**

FSW welds are very clean and strong. In comparison with conventional arc welding process, difficulties related with sensitivity to solidification cracking, softening of heat-affected zone (HAZ) and thermal distortion which are very common in fusion welding does not occur in FSW [6]. Despite its advantages, there is setback to the process. In order to run FSW, the work piece must be rigidly clamped by which that the process needs to be conducted in a very proper manner with a lot of procedures taking place. The degree of freedom for the movement of welding tool will also be very rigid and not versatile.

A major setback or defect produced by FSW on work piece is worm (tunnel) defect. It is the main target for this project. Tunnel defects (voids) and cracks may form in the welds in aluminum alloys if a judicious selection of the welding parameters is not done properly [7]. It will have a significant influence on the strength of welded structures. Figure 1.4 illustrates the presence of exit hole in FSW which is another disadvantage of this technique. The exit hole appears because of the space the welding tool previously occupied when exiting the aluminum alloy plate as the welding process ends. It also shows that the occurrence of wormhole defect (classified as void defect) appears only at the advancing side (AS) of the weld line.

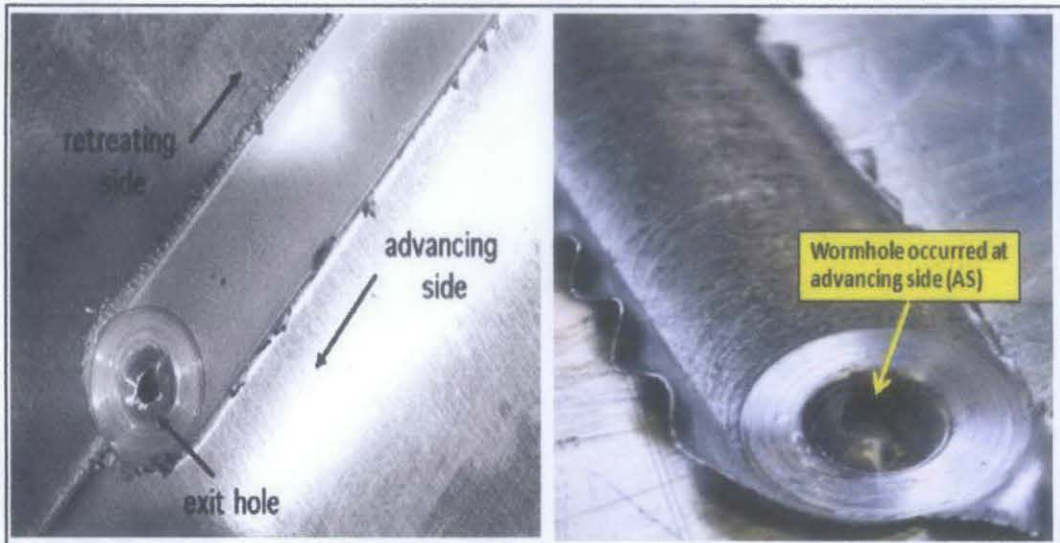


**Figure 1.4: A Friction Stir Welding (FSW) Weld between Aluminum Sheets (Left) [6] and wormhole formation indicated in Aluminium Alloy Plate (right)**

## **1.2 Problem Statement**

The problem is finding the welding parameter combination which will yield a defect free welding at the butt joined aluminum alloy plates. The welding parameter influencing weld quality includes tool spindle speed (rpm), transverse speed (mm/min), plunging speed (mm/min) and depth of penetration (mm). The presence of worm (tunnel) defect in aluminum alloy friction stir welded plates will affect the strength of the welded material. The worm defect may interfere with the welded joint ability of material to withstand forces causing stresses such as tensile, compression, bending, torsion and shear.

## **1.3 Objective**

The objective of this project is to study and examine the worm (tunnel) defect of butt welded aluminum alloy plates by adjusting the welding parameters.

## **1.4 Scope of Study**

The study will be focusing on the worm (tunnel) defect formation on butt-welded plate welding configuration. Butt-welded plate is joining edges of two (2) plate in a same plane. The material that will be used is as the workpiece is 6061 Series Aluminum Alloy Plate (100mm x 100mm x 10mm). Aluminum alloy are much lighter and have higher corrosion resistant than carbon steel [9]. Aluminum alloy classification is established by International Alloy Designation System (IADS) [10]. As for the welding tool, American Iron and Steel Institute (AISI) H13 Tool Steel Grade with tapered pin tool design was used. The welding tool was designed using AutoCAD 2007 and then fabricated using BridgePort PowerPath 15 (CNC Lathe Machine). Heat treatment was done to the welding tool to increase the hardness level. The necessary welding parameters that will be varied in this process are welding tool spindle speed (rpm) and transverse speed (mm/min) while maintaining the plunging speed (mm/min), dwell time (s) and depth of penetration (mm) at constant values. Furthermore, it is also important to possibly make suggestions and recommendations on how to reduce the magnitude of the defect, and if not, eliminating it completely.

The welding process was completed using BridgePort VMC 2216 (CNC Milling Machine). At the completions of every FSW run, the welded aluminium plates were properly labelled for further analysis, which was by using Optical Microscope (OM) and Microhardness Testing Machine. Prior to sample analysis, sample preparation procedures such as sectioning, mounting, grinding and polishing of all samples was done according.

## CHAPTER 2

### LITERATURE REVIEW

Friction Stir Welding (FSW) was invented at The Welding Institute (TWI) of the United Kingdom in 1991. Despite the advantages it has compared to other conventional welding techniques, it has a major disadvantage which is the presence of worm (tunnel) defect. The defect will form a type of void (empty space) at the welded region and it will have a significant influence on the strength of welded joint. Based on a study by Rui M. Leal and Altino Loureiro [7], tunnel defects (voids) and cracks may form in the welds in aluminum alloys if a judicious selection of the welding parameters is not being done. According to Ahmad Nordin F.A. [8], the welding parameter influencing weld quality includes tool spindle speed, transverse speed, plunging speed and depth.

Common defects in friction stir welds include porosity and surface defects. At a constant rotational speed, an increase in the travel speed leads to wormhole initiation near the bottom of the weld. Furthermore, the size of the wormholes increases with the travel speed because of inadequate material flow towards the bottom of the weld [11]. Throughout studies that have been carried out regarding the matter, there are indications that the ratio of travel speed (S) to rotational speed (N) is an important variable in the formation of the wormhole defect [12]. According to X. Long and S.K. Khanna, for the same material and tool geometry, a high ratio welding tool transverse speed (S) to spindle speed (N) tends to favour the formation of wormhole defects [13]. For example, travel speed (S) to rotational speed (N) ratio of 1: 700 is higher than ratio of 1: 1000.

Tool design and welding variables affect materials flow patterns. However, no specific character of the material flow has been related with the porosity formation and no unified mechanism of porosity formation exists. The selection of tapered pin design for the H13 Tool Steel is based on the previous studies on the tool pin geometry in FSW process by Faizul Azizi [8]. Zhao et al. [14] studied the effect of tool pin design on the weldability and mechanical properties of welded 2014 Aluminum Alloy Plates. Cylindrical and tapered tool pins did not ensure effective mixing in the vertical direction leading to wormholes at the base of the thermo mechanically affected zone (TMAZ). However, when tapered tools with threads were used, defect free welds were obtained.

Other studies by H. Schmidt and J. Hattel [15] have also confirmed that tools with screw threads generate more heat and improve flow of the softer material by exerting a downward force. Since the material flows mainly on the retreating side, insufficient plasticity and material flow results in a “wormhole” on the advancing side. The effect becomes more prominent at low temperatures due to sluggish flow of materials. Most of the heat generation occurs at the interface between the tool shoulder and the work-piece. Significant heterogeneity in heat generation at that interface can lead to defect formation in the form of excess flash due to surface overheating [11]. According to Zhao et al [14], the propensity for cracks or voids increases with the welding speed although there is an alloy-dependence. The defects tend to occur on the advancing side where an abrupt microstructural transition occurs from the highly refined nugget zone to the TMAZ while the transition was gradual on the relatively defect-free retreating side.

Elangovan et al. [16] examined the effects of rotational speed and tool pin design on defect formation in friction stir processing of 2219 Aluminum Alloy. Five pin profiles (straight cylindrical, tapered cylindrical, threaded cylindrical, triangular and square) were used to fabricate joints at various tool rotational speeds. The square tool pin profile produced the least defect content in the weld as the flat faces produced a pulsating action which led to more effective stirring. Also, a square tool has higher eccentricity which is defined as the ratio of the dynamic volume swept by the tool to the static volume of the tool.

In FSW lap joints of AA5083 and SS400, the size of the wormhole (voids) formed along the weld interface increases with the increase in diameter of the tool pin and tool tilt angle [17]. Large diameter pin (>5mm) produces more heat and forms intermetallic compound FeAl<sub>3</sub> and Fe<sub>2</sub>Al<sub>5</sub> instead of FeAl formed at lower temperature. Aluminum rich FeAl<sub>3</sub> and Fe<sub>2</sub>Al<sub>5</sub> are harder and more brittle. Table 2.1 shows the various tool designs from The Welding Institute (TWI).

**Table 2.1: Selection of Tool Design at The Welding Institute (TWI) [6]**

Tool	Cylindrical	Whorl™	MX triflute™	Flared triflute™	A-skew™	Re-stir™
Schematics						
Tool pin shape	Cylindrical with threads	Tapered with threads	Threaded, tapered with three flutes	Tri-flute with flute ends flared out	Inclined cylindrical with threads	Tapered with threads
Ratio of pin volume to cylindrical pin volume	1	0.4	0.3	0.3	1	0.4
Swept volume to pin volume ratio	1.1	1.8	2.6	2.6	depends on pin angle	1.8
Rotary reversal	No	No	No	No	No	Yes
Application	Butt welding; fails in lap welding	Butt welding with lower welding torque	Butt welding with further lower welding torque	Lap welding with lower thinning of upper plate	Lap welding with lower thinning of upper plate	When minimum asymmetry in weld property is desired

According to A.P. Reynolds [18], the wormhole or tunnel defect is a volumetric defect that may or may not be continuous. In some cases, the tunnel defect may be surface breaking. Defect location depends on the alloy and the welding condition but is normally on the advancing side of the weld. It will occur at either in the region where pin and shoulder flow regimes intersect (typically from hot welds) or near the root (usually under cold welding conditions or high advance per revolution). Mitigation is by tool design or weld parameter modification. The occurrence of wormhole defects is more difficult to contain and control in material with high hot strength and low thermal conductivity. Based on a study by I. Valavanis & D. Kosmopoulos [19], some of the most common weld defects that can be identified in the radiographic images are the worm holes (worm-like cavities), slag inclusion (slag or other foreign matter entrapped during welding), linear porosity (linear cavities due to entrapped gas), gas pores (spherical cavities due to entrapped gas), lack of fusion (lack of union between weld and base metal) or cracks which are discontinuities form by metal fracture.

According to R.M. Leal et al [20], defects in friction stir welds have already been classified as flow or geometric related. The geometric related defects are usually associated with lack of penetration (LOP) and occur due to insufficient pin penetration depth and/or improper seam tracking. The flow related defects, which are much more difficult to avoid includes flash formation, surface galling, lack of fill, wormholes (tunnel defect) and nugget collapse or lack of consolidation. The main process parameters influencing material flow and weld quality include tool geometry (pin and shoulder design and relative dimensions of pin and shoulder), welding parameters (tool rotation rate and direction, traverse speed, plunge depth, tilt angle), base material flow stress behaviour and temperature as well as the interaction between the work piece material and the various weld tool features.

Based on a study by K. Kumar & S. Kailas [21] on the role of FSW tool on material flow and weld formation, the material flow is layer wise flow in pin-driven region and bulk flow in shoulder-driven region. From the study, it is understood that a defect-free weld form when the shoulder-driven material merges with pin-driven material. It requires adequate temperature and hydrostatic pressure. It can be seen that when the shoulder-driven material does not reach the advancing side of the weld, this condition will produce the groove like defect in the weld. As the axial load increases, the shoulder interaction increases, the shoulder-driven material progressively moves towards the advancing side and bonds with its base. During this process, the material near the surface reaches the advancing side earlier and bonds with base material. The main cause for these defects is insufficient material to fill the cavity. If the shoulder is not capable of confining the transferred material within the weld cavity, a part of the transferred material is lost as flash. Hence, the shoulder-driven material is not enough to fill the cavity and this leads to the groove and void like defects in the weld. If the weld cavity is not filled completely, the required hydrostatic pressure cannot be generated. It will lead to lack of bonding between the layers. When the shoulder interaction increases, flash material reduces and shoulder-driven material will merge with both pin-driven material and base material.

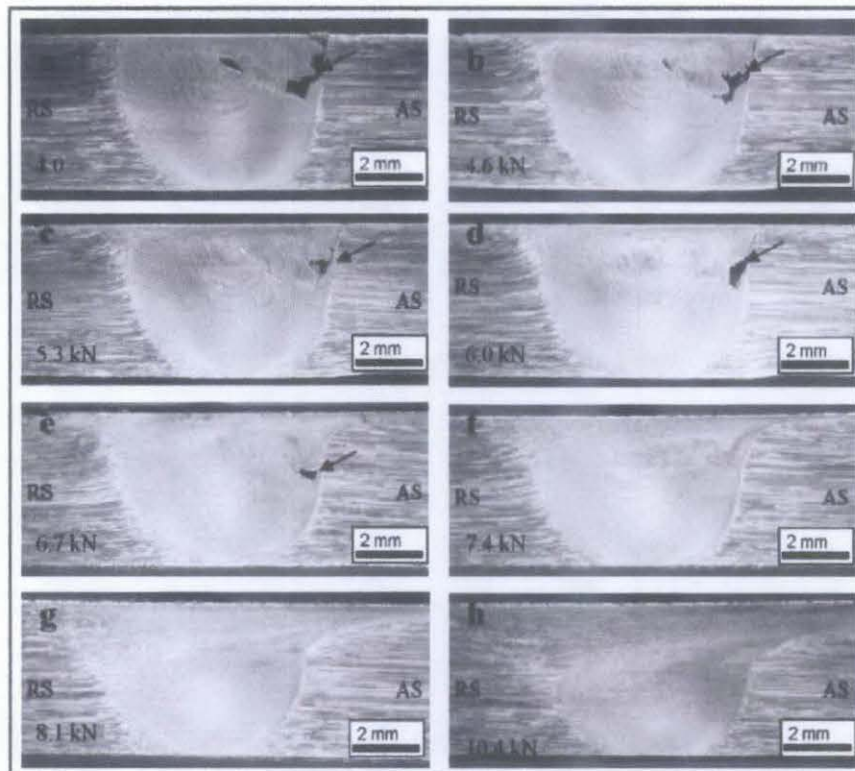


**Figure 2.1: Evolution of a Defect-Free Weld as a Function of the Shoulder Interaction with the Base Material. Arrow Marks Indicate The Presence of Voids In The Weld [21].**

Figure 2.1 is the result from the study by K. Kumar & S. Kailas [21] which shows different wormhole size by different load force applied on the welding tool. According to a study by W. V. Haver et al [22], typical welding defects encountered during the welding parameter optimization phase was crack appearing in the TMAZ on the retreating side (RS). The phenomenon can be explained as the result of the presence of flaws (pores), or which in other words that goes with this project, wormhole defect in the material microstructure in combination with its very low deformability. Tunnel defects or voids in the weld nugget on the advancing side (AS) is another feature or defects that is common FSW with non-optimised welding parameters due to inappropriate material flow. Porosity (wormhole) can be found in immersed friction stir welds as the bubbles create voids in the nugget and TMAZ. It is analogous the fusion welding done in inert gases in which the weld pool dissolves gas into it inducing porosity during resolidification. In general, there is no porosity in FSW at low rotation and travel speeds due to the solid state process [23].

## CHAPTER 3

### METHODOLOGY

In order to achieve the objective of this project, there are many steps involving the FSW operation and for the preparation to study and examine the worm (tunnel) defect of the welded region.

#### 3.1 AISI Tool Steel H13

Tool steel refers to a variety of carbon and alloy steels that are mainly well-suited to be made as welding tool. The primary functions of tool steels is for fabricating tools used in manufacturing and for the working and forming of metals, plastics, wood and other industrially used materials. The properties that qualify tool steels for tools and dies are resistance to wear, stability during heat treatment, strength at high temperatures and toughness [24]. Tools also must withstand high specific loads which often concentrated at exposed areas. It is continuously in contact with abrasive types of work materials and are often subjected to shocks or may have perform under other varieties of adverse conditions.

Tool steels are increasingly being used for mechanical parts to reduce size or weight, or to resist wear or high-temperature shock. In order to develop their best properties, tool steels are always heat treated. Because the parts may distort during heat treatment, precision parts should be semi finished, heat treated, then finished. Nevertheless, in conditions where the tool steel is regarded be subjected at normal operating conditions, it should not suffer major damage, untimely wear resulting in the dulling of edges, or be susceptible to detrimental metallurgical changes. Tools for less demanding uses, such as ordinary hand tools, including hammer, chisels, files and mining bits are often made of AISI steels that are not considered as belonging to any of the tool steel categories. The steel for most types of tools must be used in a heat-treated state, generally hardened and tempered to provide the properties needed for the particular application. The adaptability to heat treatment with a minimum of harmful effects, which dependably results in the intended beneficial changes in material properties, is still another requirement that tool steels must satisfy [25].

The selection of H13 Tool Steel as the material for welding tool is because it is categorized as hot work tool steel (Type H), serves well at elevated temperatures and commonly used for aluminum alloy. H13 combines good red hardness and abrasion resistance with the ability to resist heat checking. The tungsten and molybdenum high-alloy hot-work steels are heat and abrasion resistant even at 600 to 1,000°F [26]. The hardness, resistance to abrasion, ability to hold a cutting edge and resistance to deformation at elevated temperature are all the important characteristics of tool steel. The H13 is classified by American Iron and Steel Institute (AISI). The welding tool serves three (3) primary functions, which are heating of the workpiece, movement of material to produce the joint, and containment of hot metal beneath the tool shoulder. Tool steel H13 is used for more hot work tooling applications than any other tool steel. It is also used in a variety of cold work tooling applications because of its high toughness and very good stability in heat treatment. In these applications, H13 provides better hardenability (through hardening in large section thicknesses) and better wear resistance than common alloy steels such as 4140 [26]. Table 3.1 shows the chemical composition of AISI H13 Tool Steel.

**Table 3.1: Chemical Composition of AISI H13 Tool Steel [26]**

<b>Element</b>	<b>Weight %</b>	<b>Weight % From Supplier's Material Certification</b>
Carbon (C)	0.32-0.45	0.393
Manganese (Mn)	0.20-0.50	0.34
Silicone (Si)	0.80-1.20	1.03
Chromium (Cr)	4.75-5.50	5.02
Nickel (Ni)	0.30	-
Molybdenum (Mo)	1.10-1.75	1.27
Vanadium (V)	0.80-1.20	0.94
Copper (Cu)	0.25	-
Phosphorus (P)	0.03	0.023
Sulphur (S)	0.03	0.001

### 3.2 Fabrication of Welding Tool using CNC Lathe Machine

The welding tool will be fabricated using BridgePort PowerPath 15 (CNC Lathe Machine) and undergo heat treatment. The welding process will be using BridgePort VMC 2216 (CNC Milling Machine). It is designed to use modern carbide tooling and fully utilize modern processes. The machine is controlled electronically via a computer menu style interface. The program can be modified and displayed at the machine along with a simulated view of the process. The operator needs a high level of skill to execute the process. Even so, the knowledge base is broader compared to the older production machines where intimate knowledge of each machine was considered an important element [9]. The pin length depends on the thickness of the workpiece, the tool tilt and the desired clearance between the ends of the pin and the anvil. The depth penetration of the pin of welding tool can only be done 80% from the thickness of workpiece [2]. In this project, the workpiece have a thickness of 10mm which means that the pin length should be designed and fabricated to 8mm. Figure 3.1 shows the design of the Tool Steel using AutoCAD 2007 software.

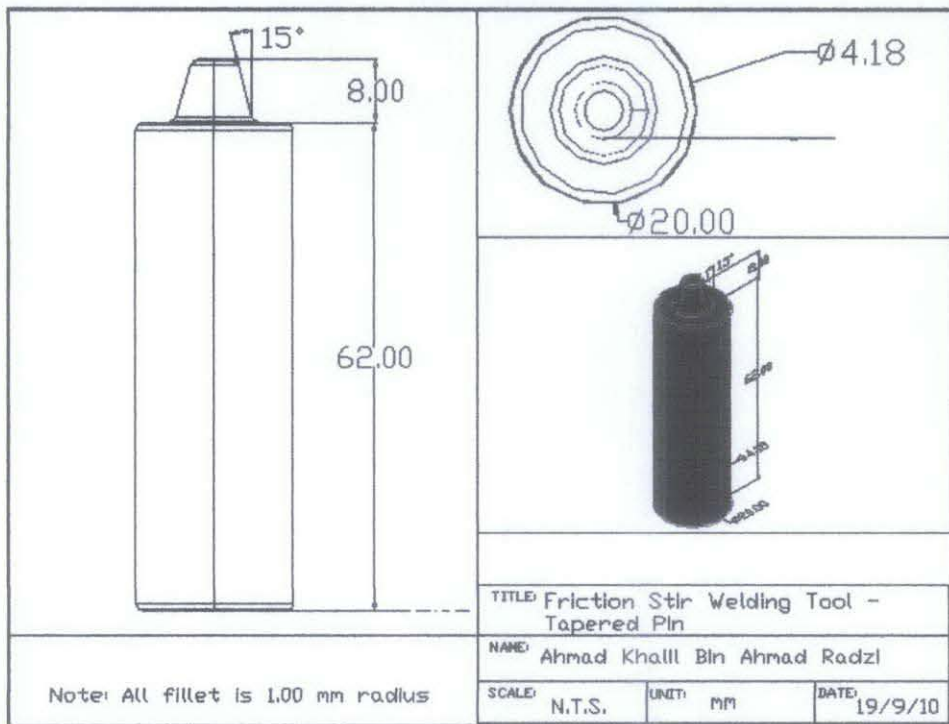


**Figure 3.1: Design of Cylindrical Tapered Pin H13 Tool Steel using AutoCAD 2007**

### **3.3 Work piece Preparation**

The workpiece that will be used for this project are aluminum alloy. The aluminum alloy can be obtained from Mechanical Engineering Building 21. The dimension of the workpiece will be 100mm x 100mm x 10mm. Prior to the welding process, there are several activities that need to be fulfilled before the project can proceed any further. Since the aluminum alloy does not come with its designated material certification, the author needs to verify the material composition for the Aluminum alloy plates by running specific material characterisation test method which is Field Emission Scanning Electron Microscope (FESEM). The machine is available at the Postgraduate (PG) Research Building.

### **3.4 Heat Treatment of AISI H13 Tool Steel**

In line with the welding tool preparation, the tool steel will be heat treated to produce a great variety of microstructures and properties. Generally, heat treatment uses phase transformation during heating and cooling to change a microstructure in a solid state. In heat treatment, the processing is most often entirely thermal and modifies only structure. Thermomechanical treatments, which modify component shape and structure, and thermochemical treatments which modify surface chemistry and structure, are also important processing approaches which fall into the domain of heat treatment. The heat treatment was done by using CARBOLITE Heat Treatment Tube Furnace as shown in Figure 3.3. It is located at Mechanical Building 17. The procedures for the H13 Tool Steel heat treatment process are as below [8, 9] and is shown in a graphical form as in Figure 3.2:

1. The welding tool is inserted into the Tube Furnace and preheated initially for two (2) hours to rise from 30°C to 732°C.
2. Next, the preheating of welding tool continues slowly from 732°C - 760°C for another two (2) hours.
3. The temperature will be raised to 1000 °C for one (1) hour.
4. Finally, it will be cooled down to 30°C for two (2) hours.

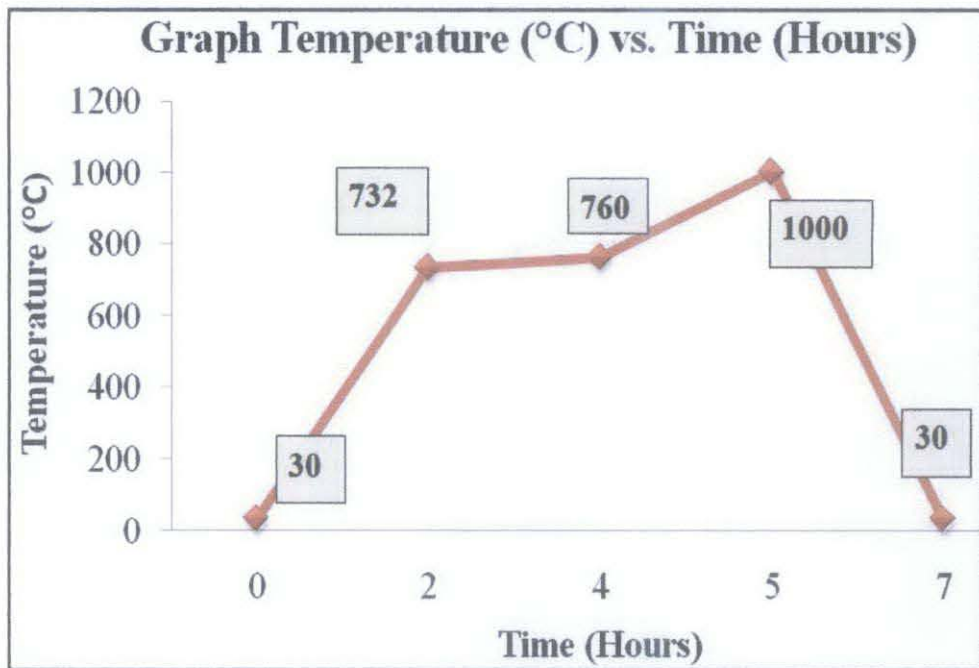


**Figure 3.2: Temperature Profile during the Heat Treatment Process**



**Figure 3.3: Carbolite Tube Furnace**

### 3.5 Hardness of Tool Steel

As the fabrication of the welding tool is completed, the hardness reading of the tool is taken before it undergoes heat treatment process. It is to prove that the hardness will increase after undergoing heat treatment. The hardness test was done using the Rockwell Hardness Test Machine at Mechanical Engineering Building 17 (Material Laboratory). The Rockwell Hardness Test ranges from Rockwell A to G.

For this project, we are using Rockwell C which uses a diamond cone type indenter and with 150 kg load as shown in Figure 3.4 [27]. The Rockwell Hardness value for H13 Tool Steel should be in the range of HRC 38-55.



**Figure 3.4: Hardness of Tool Steel taken using OMAG Brevetti Affri Hardness Testers**

**Table 3.2: Hardness Reading of Welding Tool Steel H13 Before and After Heat Treatment Process**

Readings	Rockwell Hardness (HRC)	
	Before Heat Treatment	After Heat Treatment
1	33.0	49.1
2	33.3	45.0
3	32.5	45.9
4	33.5	46.2
5	34.2	45.5
6	32.5	43.3
7	33.3	42.6
8	33.5	47.1
9	33.0	44.5
10	33.4	48.3
<b>Total</b>	<b>332.2</b>	<b>457.5</b>
<b>Average</b>	<b>33.22</b>	<b>45.75</b>

Thirteen (13) readings were taken throughout this process. The first three (3) readings were ignored and the average of the tool steel H13 hardness before heat treatment is measured to be 33.22. After the heat treatment on the tool steel is done, hardness is calculated to be 45.75. The results are shown in Table 3.2. The hardness of tool steel is increase by 38% due to heat treatment process. Figure 3.5 shows the physical state of the H13 Tool Steel before and after heat treatment. The process results in the change in color of the tool surface compared to its original state.



**Figure 3.5: The Raw H13 Tool Steel (Left) and Finish Product after Heat Treatment (Right)**

### **3.6 Friction Stir Welding Process**

Figure 3.6 shows that the welding tool is set up onto the “BridgePort VMC 2216” Milling Machine together with the computerized programming codes. Since undergraduates are not allowed to operate the machine by themselves, the FSW process is assisted by Mechanical Engineering Lab Technician, Mr. Shaiful Hisham. The 6061 aluminum alloy plates is joined together by using the tool steel H13 and by varying different combination of welding parameters which is the transverse feed rate (mm/min) and spindle speed (rpm). The aluminum alloy plates needed to be drilled with holes in order to attach it to the welding jig using set of bolts and nuts before it is able to undergo the welding process.

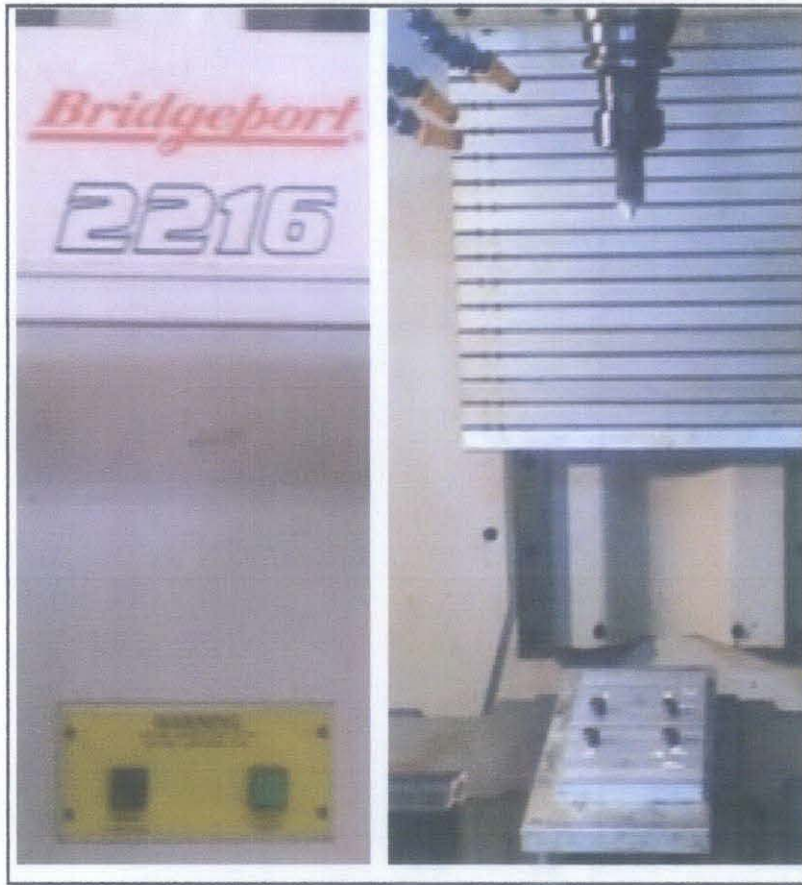


**Figure 3.6: FSW Run is completed using BridgePort VMC 2216  
(CNC Milling Machine)**

### **3.7 Sample Preparation**

At the completion of welding process, aluminum alloys requires the same principle of sample preparation for examination as most metal does. The fracture surfaces must be carefully preserved against abrasion or contamination. If the part is difficult to handle and has to be sectioned, care should be taken to cut the material along directions determined by the working process and by other interesting criteria. As an example, if the alloy has been rolled, it can be interesting to examine the evolution of microstructure along the rolling direction and so the part must be cut in the same direction.

The general metallographic sample preparation for optical microscopy includes a series of steps described in the following paragraph. The selected part of the material is cut by a silicon carbide (SiC) abrasive saw at a certain distance from the plane to be observed, because a thickness of several tens of microns will be then removed by mechanical grinding. A lubricant for cutting is used to control temperature increases and structure modification of the specimen. The sectioning is usually followed by mounting of the sample in a plastic medium to form a cylindrical piece that can be handled during grinding and polishing. [28]

### 3.7.1 Sectioning

Sectioning is done because of the size limitation of specimen to be mounted using the Auto Mounting Press Machine. The machine can only fit a certain area size range of a sample. An abrasive non-ferrous cutter was used for the sectioning process and the intended area to be examined is the welded area region. The abrasive cutoff disc is usually made from silicon carbide particles, or diamond particles (called diamond saws). From the welded sample, the cross section of the sample was taken into account. The sectioning process was first done using Linear Hack Saw machine as shown in Figure 3.7 After the samples were cut to be at a certain thickness range, only then it is further sectioned using non-ferrous abrasive cutter machine as shown in Figure 3.8 for more precise an accurate sectioning. Labeling of all sectioned sample is important so that we can keep track of the welding parameters that a particular welding section had undergone without mixing it with other sections.



**Figure 3.7: Sectioning of Aluminium Alloy Plates using KP-280 Linear Hack Saw Machine**



**Figure 3.8: Delta Non-Ferrous Abrasive Cutter**

### **3.7.2 Mounting**

After sectioning process is the mounting process. Mounting is required when sample is small or oddly shaped for subsequent handling and metallographic polishing. Specimen mounting allows for convenient handling of various shapes and sizes during the subsequent preparation and examination. Hot compression mounting minimizes shrinkage, protects and preserves edges and surface defects during preparation steps and provides excellent sample quality. Compression mounting provides a predictable and convenient size and shape and allows specimen information to be marked on the backside for record keeping [29].

The examined sample is mounted in a thermoset plastic material (BUEHLER Phenolic Powder Black) shown in Figure 3.9. It is classified as hot mounting process. The mounting parameters are dependent on the type of Phenolic Powder that is being used and were preset by the technicians. The stages (cycles) of mounting process are pressurizing, pre-heating, heating and cooling. Mounting parameters involved are:

- Heating Time – 3 minutes
- Cooling Time – 2 minutes
- Pressure Applied – 4000 psi



**Figure 3.9: BUEHLER Auto Mounting Press Machine [29]**

### **3.7.3 Grinding and Polishing**

The next step is the grinding process using MetaServ 200 Grinder Machine. The objective of grinding is to remove the damages on the surface produces by sectioning. Grinding also produces damages which must be minimized so that subsequent are grinding with finer abrasives. At the end of the grinding phase, the remaining damages present will be removed by polishing [28]. The grinding material used is abrasive paper covered with silicon carbide grits as shown in Figure 3.10. It is commonly a series of abrasive paper from coarse to fine one. Figure 3.11 shows that the lubricant used is water and the rotational speed for the grinding machine is fixed at 200 rpm. The grit sequence for the grinding process is 180, 240, 320, 400, 600 and 1200. For the polishing process, 3 micron diamond paste is used to have mirror-liked image at the surface of specimen.



**Figure 3.10: BUEHLER Special Silicon Carbide Grinding Paper**



**Figure 3.11: Grinding Process of Mounted Aluminum Alloy Sample with Water as Lubricant**

### 3.7.4 Etching

Additional surface treatments such as chemical etching can improve the contrast between microstructural constituents of a polished section. Due to the nature of aluminum alloy being ductile and soft, it is difficult to prepare by mechanical polishing. The etchant used in this process is Keller's Reagent, which is the most widely used etching reagent in most research for aluminum alloy according to ASM Handbook Volume 9 [9]. Chemical composition for Keller' Reagent is as follows:

- 190 ml of water
- 3 ml of hydrochloric acid (HCl)
- ml of nitric acid (HNO<sub>3</sub>)
- 2 ml of hydrofluoric acid (HF)

### 3.8 Wormhole Size Measurement

The wormhole size of all the samples was measured using the manual measurement option that is available together with the Optical Microscope (OM) shown in Figure 3.12. Initially, the plan was to use the Non-Contact Measurement Machine to measure the defect size but the machine have the limitation of only measuring areas in geometric shape such square, circle, rectangle etc. Even though the area can be estimated through this technique, the result will not be desirable. Meanwhile, the Optical Microscope has the ability to measure areas of all shape profile. The technique was to trace the parameter of the worm defect and it will calculate the area in the unit of micrometer squared. Since the machine goes in the

microscopic level images, it is unable to capture the full image of the worm defect. In order to solve this problem, I had to measure each one of the twenty seven (27) part by part to get the full area.

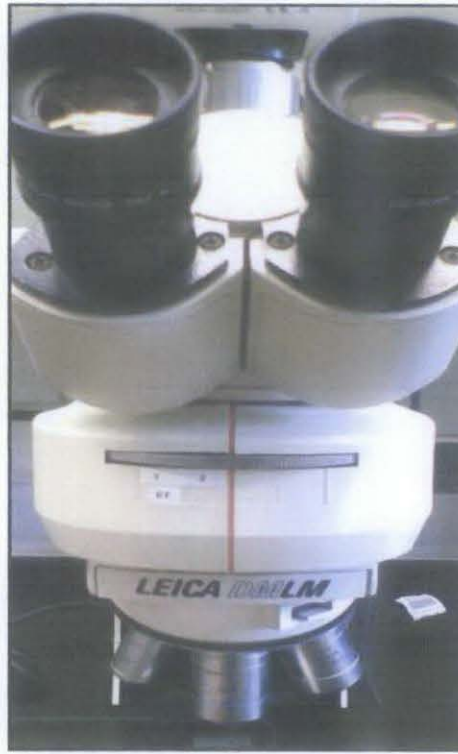


**Figure 3.12: Leica DMLM Optical Microscope**

### **3.9 Vicker Microhardness Testing**

Hardness is a commonly used property that gives a general indication of the strength of the material and its resistance to scratching and to wear. Hardness can be defined as resistance to permanent indentation. The resistance to indentation depends on the shape of the indenter and on the load applied [27]. For this project analysis, we will be using the Vickers hardness test method, also referred to as a microhardness test method. The method is mostly used for small parts, thin sections, or case depth work. It is based on an optical measurement system. Figure 3.13 shows the illustration of Brinell Hardness Test using ball shape indenter. Directly below the indentation, the density of particles is forced to increase, compared to regions away from the depression. As the indenter moves downward during the test, it encounters resistance from a material with an increasingly greater concentration of hard particles [30]. The understanding is that the larger the indent mark on a sample surface, the lower the hardness level of a particular material.

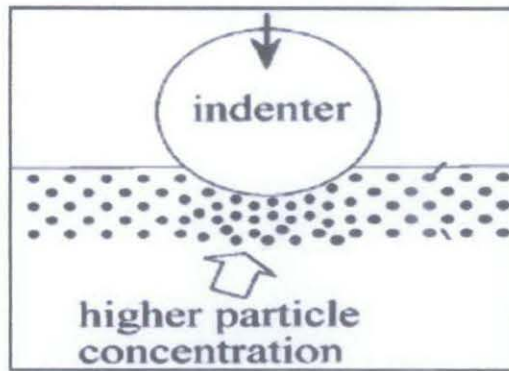


**Figure 3.13: Schematic Illustrating the Local Increase in Particle Concentration Due To Indentation [30]**

The Microhardness test procedure, ASTM E-384, specifies a range of light loads using a diamond indenter to make an indentation which is measured and converted to a hardness value. Here, a square based pyramid shaped diamond is used for testing in the Vickers scale. Prior to the microhardness test shown in Figure 3.14, sample preparation is usually necessary in order to provide a small enough specimen that can fit into the tester. Furthermore, the sample preparation will need to provide a smooth surface of specimen to allow regular indentation shape and good measurement. It is also to ensure the sample can be held perpendicular to the indenter [31].



**Figure 3.14: The Vicker Microhardness (HV) of Prepared FSW Sample is taken using LECO LM247AT Microhardness Testing Machine**

### **3.10 Key Milestones**

Below is the key milestone that is being complete throughout the project. Figure 3.15 shows the overall project work flow for FYP II.

The key milestones completed for FYP I are listed below.

- 1) Completion of H13 Tool Steel design, fabrication and heat treatment process. (Week 7)
- 2) Completion of the trial run for the welding process using “BridgePort VMC 2216 (CNC Milling Machine). (Week 13)

The key milestones completed for FYP II are listed below.

- 1) Completion of all FSW run of welding process onto the Aluminum alloy plates with the tool steel H13 and by varying different combination of welding parameters which is the transverse feed rate (mm/min) and spindle speed (rpm). (Week 1)
- 2) Completion of wormhole size measurement and micro hardness testing on all welding samples and investigates the relationship with the size of worm defect. (Week 10)
- 3) Completion of report and investigation on the relationship with the size of worm defect. (Week 13)

### 3.11 Project Work Flow (FYP II)

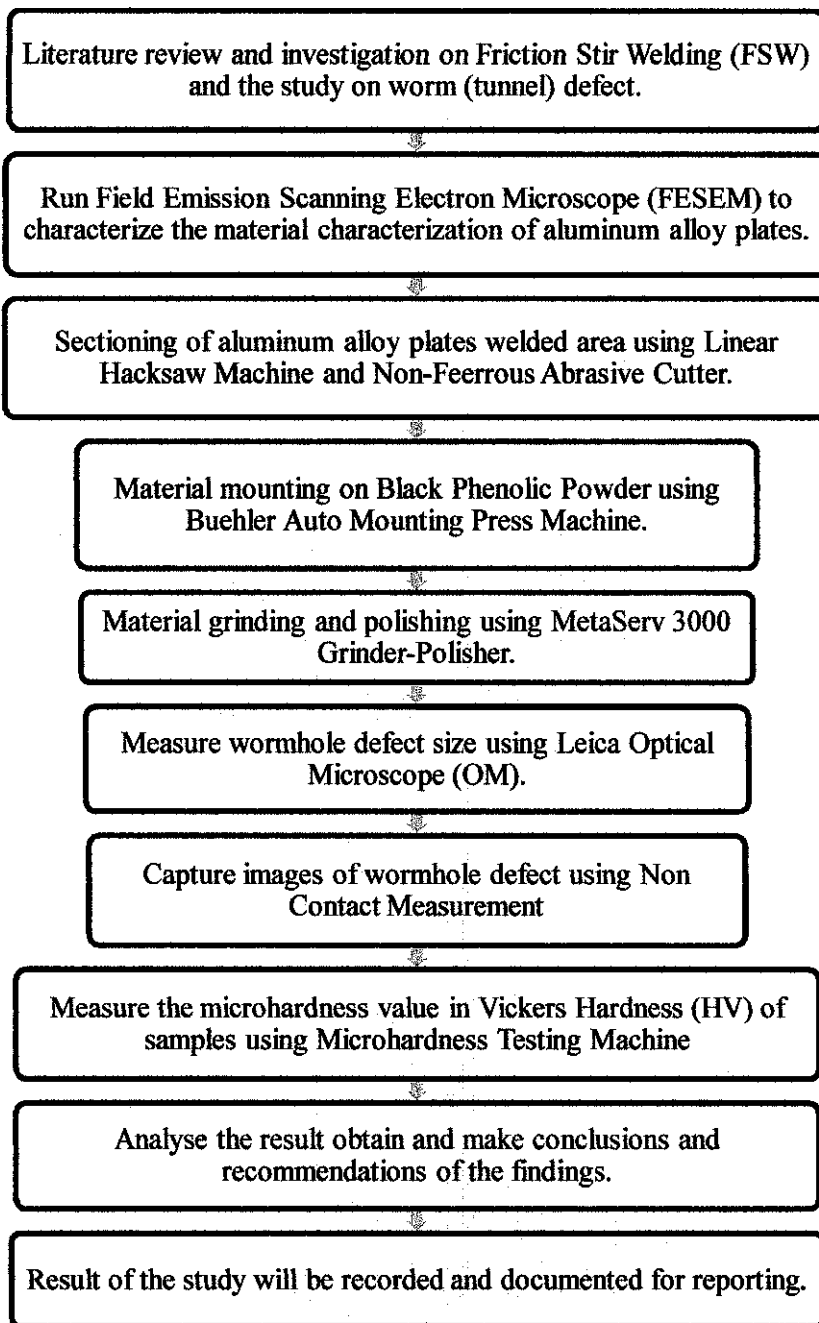


**Figure 3.15: Project Work Flow (FYP II)**

## CHAPTER 4

### RESULTS AND DISCUSSION

In this chapter, related results are being documented. Here, we want to see the outcome by three (3) sets of varying combination of welding parameters and make discussion of the result.

#### 4.1 Welding Parameters

For this research, a plunging feed rate is fixed at 10mm/min and penetration rate at -8.1mm. All samples will have the same variables of transverse feed rate to spindle speed ratio (S: N) of 1:1000, 1:850 & 1:700. Table 4.1 and 4.2 shows the variation of welding parameter combination by keeping the spindle speed constant. Meanwhile for Table 4.3, the feed rate is kept constant at 50mm/min.

**Table 4.1: Constant spindle speed (N) of 1,100 rpm**

Sample	Transverse Feed Rate, S (mm/min)	Spindle Speed, N (rpm)	Spindle Speed, N (mm/min)	Ratio (S:N)
1 (X1)	34.56	1,100	34,562	1:1000
2 (X2)	40.67	1,100	34,562	1:850
3 (X3)	49.37	1,100	34,562	1:700

**Table 4.2: Constant spindle speed (N) of 2,200 rpm**

Sample	Transverse Feed Rate, S (mm/min)	Spindle Speed, N (rpm)	Spindle Speed, N (mm/min)	Ratio (S:N)
4 (Y1)	69.12	2,200	69,124	1:1000
5 (Y2)	81.32	2,200	69,124	1:850
6 (Y3)	98.75	2,200	69,124	1:700

**Table 4.3: Constant feed rate (S) of 50 mm/min**

Sample	Transverse Feed Rate, S (mm/min)	Spindle Speed, N (rpm)	Spindle Speed, N (mm/min)	Ratio (S:N)
7 (Z1)	50	1,591	50,000	1:1000
8 (Z2)	50	1,353	42,500	1:850
9 (Z3)	50	1,114	35,000	1:700

#### 4.2 Welding Results

Each sample was sectioned into three parts which is the tool entrance, middle part and tool exit. Based on observation, the size of wormhole is not constant throughout the sample. The size of wormhole which forms at the welding joint varies according to the location. From an early observation, it is found that the size of wormhole is at minimal (smallest) at the entrance part of the tool and begins to increase as the welding tool moves along the weld path on the aluminum alloy plates. The labeling of cross section of each sample FSW plates as shown in Table 4.4 and Figure 4.1:

**Table 4.4: Sectioned Wormhole Region**

Point	Note (Wormhole Region)	Distance From Entrance of Tool at the 6061 Aluminum Alloy Plate
1	Exit	65 mm
2	Middle	35 mm
3	Entrance	5 mm

Note: Total length of weld line (distance from tool entrance to exit) = 70 mm

**Figure 4.1: Weld Path with Respective Labeling**

We can see that there is presence of splash due to improper flow of material inside the friction stir zone. The excess material which creates the splash was actually the effect of material from inside the aluminum alloy plates pushing the upper material on the surface. Eventually, it will cause the formation of the wormhole. Here, we can say that the wormhole initiation is connected to splash formation. The wormhole can be clearly seen when the plates were sectioned. The next step after the grinding process is to do the polishing of each sample. It is to yield mirror like finish which will later enhance the image and result by using Optical Microscope (OM). Later through the process, etching must be done to make the image clear and easy for interpretation. During mounting process, compression of Black Phenolic Powder pushes it to enter the wormhole from the back and appears in the front surface of the specimen as shown in Figure 4.2. It is indicated by the black spot which is visible on the surface of the specimen. Here, we can analyze further regarding the size of the wormhole by using Manual Measurement Application from Optical Microscope.

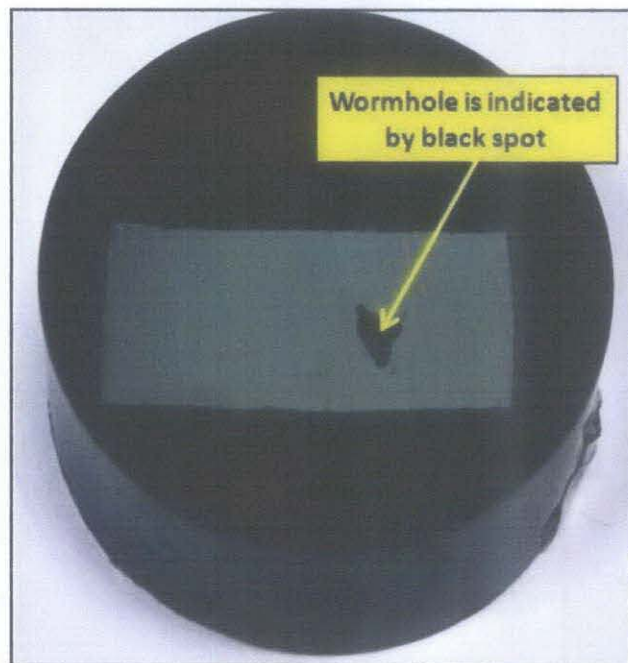


**Figure 4.2: Wormhole Defect Appears at the Grinded Sample**

### 4.3 Material Characterization

The aluminum alloy work piece has not been identified specifically. In order to quantify the origin and material properties of the aluminum alloy, Field Emission Scanning Electron Microscope (FESEM) material characterization test was run onto the work piece sample. FESEM produces clearer, less electrostatically distorted images with spatial resolution down to 1.5nm, which is 3 to 6 times better than conventional SEM.

The principle of FESEM is under vacuum condition, electrons generated by a Field Emission Source are accelerated in a field gradient. The beam passes through Electromagnetic Lenses, focusing onto the specimen. As the result of this bombardment different types of electrons are emitted from the specimen. A detector catches the secondary electrons and an image of the sample surface is constructed by comparing the intensity of these secondary electrons to the scanning primary electron beam. Finally the image is displayed on a monitor. The addition of Energy Dispersive X-ray (EDX) detector combined with digital image processing is a powerful tool in the study of materials, allowing good chemical analysis of the material [32].

The FESEM Material Test is done by using SmartSEM EDS INCA Energy Machine. The process was done three (3) times and getting the average in order to get more accurate result. The FESEM result is shown in Table 4.5 and Figure 4.3.

**Table 4.5: Elemental Analysis of the Aluminum Alloy Sample**

Element	Weight %	Atomic %
Aluminum (Al)	97.13	96.61
Magnesium (Mg)	0.86	0.95
Silicone (Si)	0.71	0.68

From the result, we can see that the total percentage of element is not 100%. It is because there is small presence of oxygen due to mishandling of sample that is still detected by the FESEM machine. From Table 4.5, there appears to be only three (3) elements in the aluminum alloy work piece. According to the Wrought Aluminum Alloy Designation System, alloys of this series are designated 6xxx. This group includes magnesium (Mg) and silicone (Si) as the major alloying elements. Bases on the percentage of magnesium (Mg) and silicone (Si), we can classify that the work piece is in the class of **Aluminium Alloy 6061 Series (Al – Mg -Si)**.

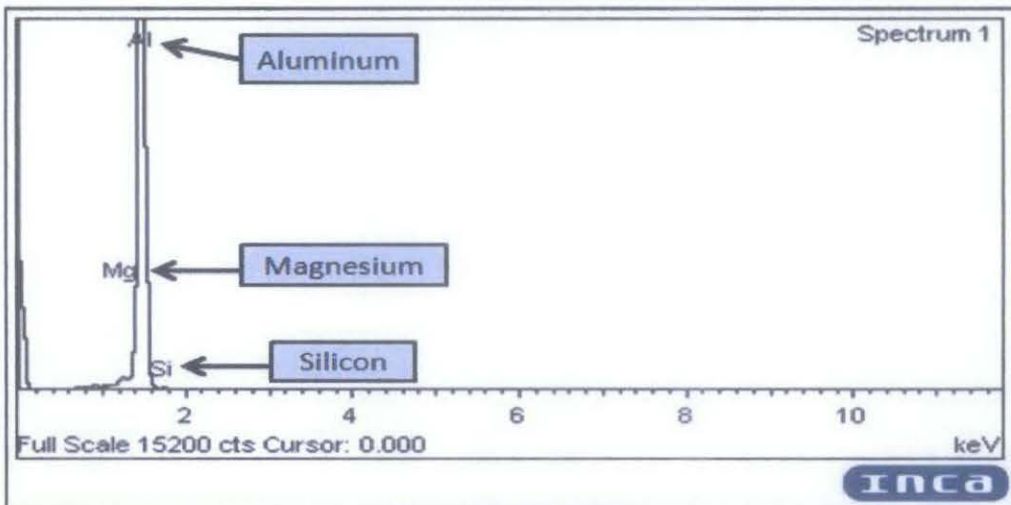


**Figure 4.3: Graphical Result of Elemental Analysis using FESEM Displayed on the Monitor**

The general characteristics of aluminium-magnesium-silicone (6xxx series) alloys are heat-treatable. Solution treatment followed by either artificial or natural aging allows considerable increasing the yield strength 3-5 times. Alloys of this series possess high mechanical strength combined with good formability and corrosion resistance. Excess of silicon enhances effect of precipitation hardening of the alloys, but decreases their ductility because of segregation of silicon at the regions of grain boundaries. The adverse effect of silicon may be diminished by addition of chromium and manganese depressing recrystallization during solution treatment. Aluminium-magnesium-silicon alloys (6xxx series) are used in aircraft and automotive applications, in architectural applications and structural material [33]. Figure 4.4 shows the SmartSEM EDS INCA Energy Machine that was used to complete the FESEM Material Characterisation process.



**Figure 4.4: SmartSEM EDS INCA Energy Machine**

#### **4.4 Wormhole Size Analysis**

A typical FSW defect is the wormhole or tunnel defect. It occurs at the advancing side (AS) of the weld line. It is a result of insufficient material transport around the tool pin to the advancing side. At the retreating side (RS), there is enough material that is being transported, and as a result, no wormhole defect appears at this region. The wormhole defect is a volumetric defect which in other words, produces a certain amount of void underneath the weld surface. Usually, it is observed by radiography but for this project, the aluminium alloy plates are being cross-sectioned and cut to parts in order to observe and measure the wormhole defect. The void is continuous throughout the weld line. The formation of wormhole defect at the advancing side can be prevented by the proper choice of welding parameters. From Figure 4.5, a common triangle-like shape is shown from the worm defect

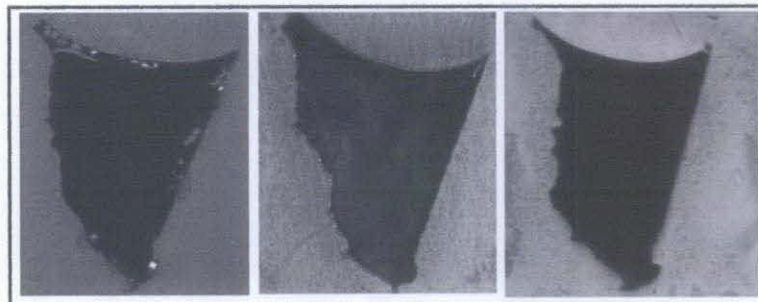


**Figure 4.5: Wormhole Images Taken using Non-Contact Measurement Machine**

Figure 4.6 shows the measurement of wormhole size by tracing the parameter with the green line. By using this option, complicated parameter profile such as curve and jagged lines can easily be traced without having to make estimation which may lead to measurement error. At the beginning of the project, it is assumed that the size of the wormhole remains constant throughout the weld line. Previous research does not show any variation regarding the wormhole size from start to finish.



**Figure 4.6: Manual Measurement of Wormhole Size using Optical Microscope**

For this project, each sample were sectioned into three (3) parts which are the entrance, middle and exit part of welding tool. From the experiment, we can see a pattern that is the size of wormhole increases from the tool entrance to the exit. It confirms with our early observation which is the size of wormhole is at minimal (smallest) at the entrance part of the tool and begins to increase as the welding tool moves along the weld path on the 6061 Aluminum Alloy plate. The reason being is because at the entrance, the tool had undergone a constant 12 s dwell time which is enough ample time to generate high temperature and having adequate material flow towards bottom of the weld.

When the welding tool moves transversely at a predetermined feed rate, the material flow towards the bottom of the weld starts to slowly decrease since the welding tool is moving from one end of the plate to another. Since the weld line is only 70 mm in length, it is not enough to say that this conclusion is valid of higher weld line that can be done for future projects. Nevertheless, the variation of wormhole size is small and is not the major focus of this project which is varying the welding parameters. In this project, a total of nine (9) samples with various combinations of welding parameters have been done by having twenty-seven (27) cross-sectioned areas for measuring of wormhole size. It means that for every sample, three (3) wormhole area values are required. For the purpose of result presentation, the wormhole area is taken as average from the entrance, middle and exit wormhole size for each sample. The result of the measured average size of wormhole is tabulated in Table 4.6 and in histogram form shown in Figure 4.7.

**Table 4.6: Results of Measured Average Wormhole Area (mm<sup>2</sup>)**

Sample	Sample Label	Average Wormhole Area (mm <sup>2</sup> )
X = <u>Constant spindle speed (N) of 1,100 rpm</u>	X1	2.64
	X2	2.97
	X3	3.09
Y = <u>(Constant spindle speed (N) of 2,200 rpm)</u>	Y1	3.91
	Y2	4.02
	Y3	6.56
Z = <u>(Constant feed rate (S) of 50 mm/min)</u>	Z1	2.38
	Z2	2.56
	Z3	2.75

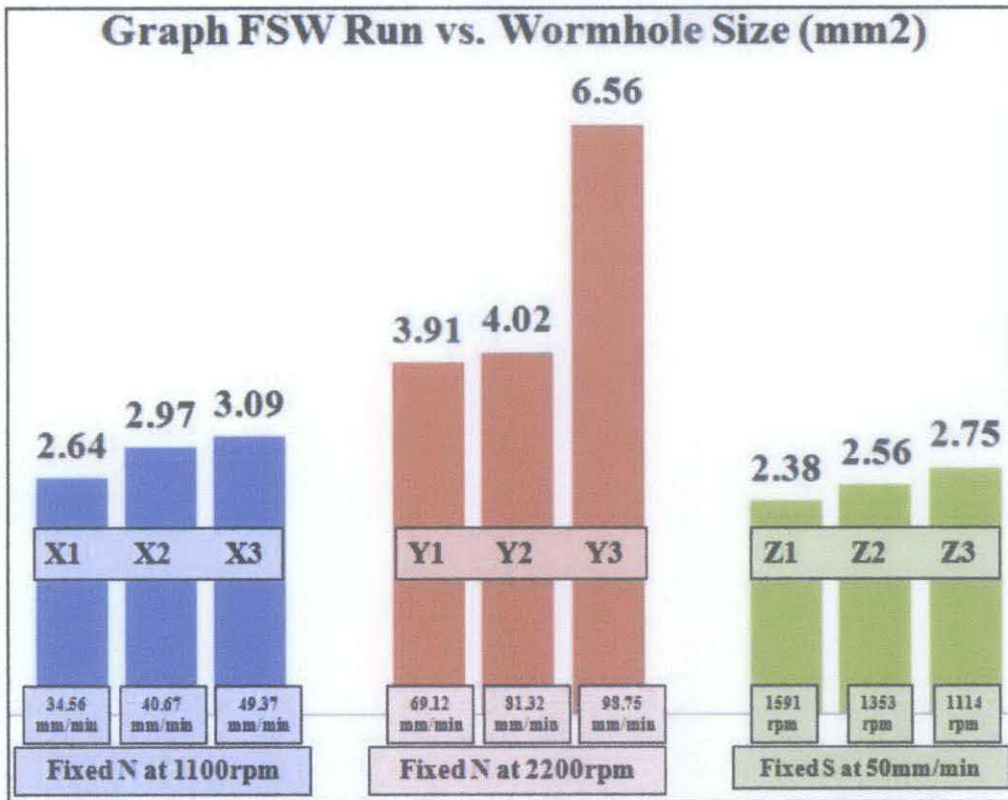


**Figure 4.7: Histogram Showing Each FSW Run with the Corresponding Size of Wormhole Cross Sectioned Area (mm<sup>2</sup>)**

Referring to Figure 4.7, it shows that at fixed tool spindle speed  $N=1,100\text{rpm}$  and  $N=2,200\text{rpm}$  (indicated by blue and red bars respectively), the increase of the (travel speed) feed rate will favor the formation of wormhole defect. The result is shown from the graph of sample X (X1, X2 and X3) and Y (Y1, Y2 and Y3) which has the same S: N ratio but sample Y is double the value of sample X welding parameter. Even though the ratio is the same, doubling the values of welding parameter will favor the formation of wormhole defect. Wormhole size increases from ratio 1:1000 to 1:700 because high ratio transverse speed to spindle speed tends to favor wormhole defect initiation.

For FSW sample Z indicated by the green bars, the ratios are still the same but here, we vary the spindle speed (rpm) while maintaining the transverse feed rate (mm/min). From Figure 4.7, it shows that FSW sample Z yields the lowest value of wormhole size (area). With that, we can conclude that the major welding parameter that affects the process of wormhole defect initiation is transverse feed rate (mm/min).

#### 4.5 Microhardness Testing

The microhardness test is taken to find the relationship between the size of wormhole that had been found out earlier and the hardness of that particular sample. For these test, samples that are being measured are from are the middle part of each FSW run. For each sample, five (5) points were marked and the hardness values were taken at these marked points. The load used is 1kN. The machine that was being used will automatically yield the value of hardness in Vickers Hardness Value (HV) without having for manual calculation using the indentation length formula. The hardness results of all nine (9) FSW sample are shown in Table 4.7.

**Table 4.7: Result of Microhardness Testing**

Sample	Retreating Side (RS)		Weld Centre	Advancing Side (AS)		Average Hardness (HV)
	-10 mm	-5 mm	0	5 mm	10 mm	
<b>Sample X</b>						
X1.2	72.9	70.5	65.9	80.3	82.0	<b>74.3</b>
X2.2	71.8	78.9	63.4	64.0	66.0	<b>68.8</b>
X3.2	67.2	65.0	60.1	69.9	72.2	<b>66.9</b>
<b>Sample Y</b>						
Y1.2	75.0	70.4	57.9	61.7	63.3	<b>65.7</b>
Y2.2	65.3	60.0	57.7	63.5	70.5	<b>63.4</b>
Y3.2	64.0	61.2	53.9	59.5	61.7	<b>60.1</b>
<b>Sample Z</b>						
Z1.2	73.9	71.5	67.1	72.4	77.0	<b>72.4</b>
Z2.2	72.7	67.3	62.8	71.3	77.4	<b>70.3</b>
Z3.2	78.2	75.1	66.3	74.1	75.5	<b>73.8</b>

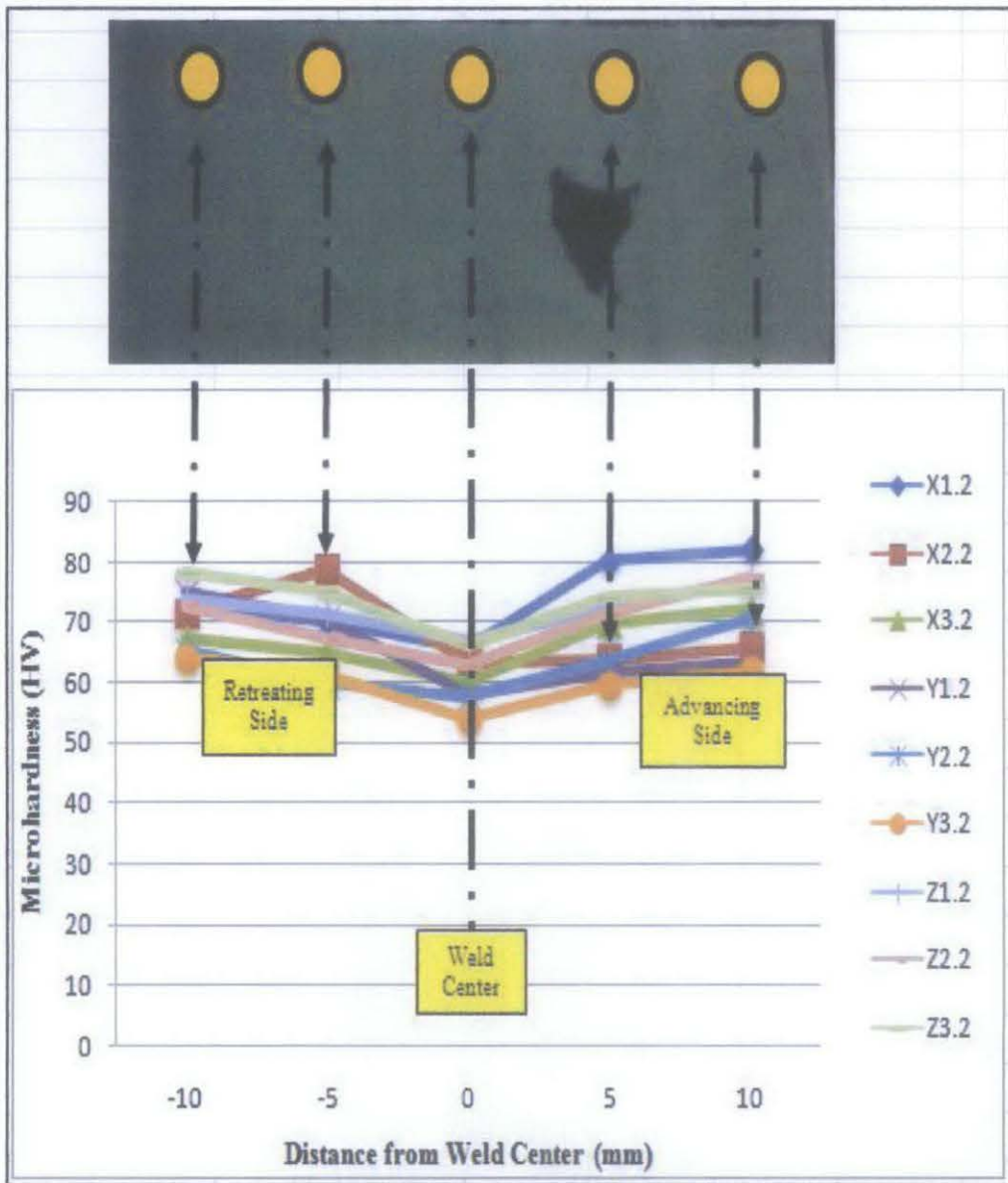


Figure 4.8: Graph Microhardness (HV) vs. Distance from Weld Center (mm)

Figure 4.8 shows that the positioning of five points for each FSW sample that were marked for the hardness values to be taken at these marked points. It is observed that the microhardness profile of the weld area corresponds on the microstructure region. The lowest value of microhardness is at the weld center. The weld center is inside the weld nugget, which is the space that was previously occupied by the welding tool during FSW process. Inside the weld nugget, the value of the microhardness drop compared to the advancing side (AS) and retreating side (RS) due to the full recrystallisation that has taken place.

From Figure 4.9 shows the relationship between microhardness and size of wormhole size. Here, we can see that as the wormhole size increases, the average microhardness (HV) of a FSW sample decreases. As the indenter moves downward during the test, it encounters resistance from a material with an increasingly greater concentration of hard particles. When there is larger void (wormhole) space in the aluminum alloy, less material is available to hold the indentation of the diamond indenter from the microhardness tester. As a result, the size of indentation on the aluminum alloy plate surface is larger and will yield a lower value of microhardness (HV). Consequently, the microhardness value increases in present of a smaller void space due to the local increase in particle concentration associated with indentation.

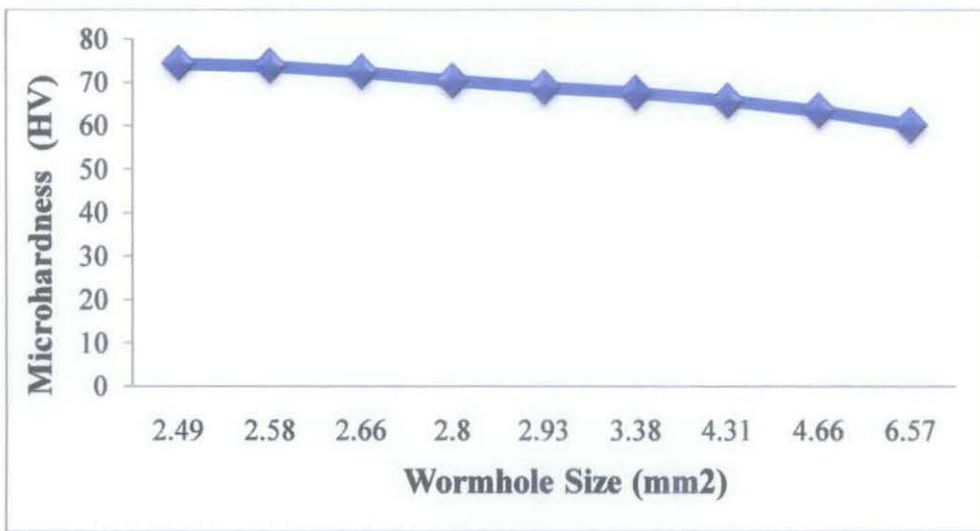


Figure 4.9: Graph Microhardness (HV) vs. Wormhole Size (mm<sup>2</sup>)

#### 4.6 Heat Generation in FSW

Heat transfer in FSW process is very important for the weld quality. The temperature history of the workpiece may determine the microstructure of the weld zone which eventually affects the welding quality history of the workpiece [34]. Here, the relationship between ratios S: N to wormhole size and microhardness is being analysed. In FSW, the heat input near the tool pin that effects the formation of wormhole defect can be calculated. The equation that is being used is  $Q = F \cdot v$  where  $Q$  = Heat Generated (Nm/s),  $F$  = Friction Force (N) and  $v$  = linear velocity (mm/min). The frictional force can be calculated by using  $F = \mu N$ , where  $\mu$  = coefficient of

friction and  $N$  = normal force applied by the tool steel on the aluminium alloy plate provided by the milling machine. The coefficient of friction depends on the local temperature and applied pressure which varies in the weld process. For this project, it is assumed that the coefficient of friction ( $\mu$ ) between aluminum (6061 aluminum alloy plate) and steel (H13 Tool Steel) is  $\mu=0.5$ . Since the milling machine used in this project does not give information on the force applied, it is assumed that normal force ( $N$ ) = 1000N for the purpose of data representation. Meanwhile, the linear velocity (mm/min) can be calculated by using the formula  $v = \omega \cdot r = 2 \pi N \cdot r$ , whereby  $\omega$  = angular velocity (rad/s),  $N$  = rotational speed / tool spindle speed (rpm) and  $r$  = tool pin radius which is 5 mm.

For this part of the project, only the data from FSW sample Z (constant feed rate (S) of 50 mm/min) will be taken. It is because from the equation, the data that affects the value of heat generated (Q) is the tool rotational /spindle speed (rpm). For data representation purposes, data from FSW Run X and Y is not taken because both of this FSW Run is having constant rotational /spindle speed (rpm) by which the result pattern will not be seen. Table will present the relationship of ratio (S: N), Heat Generated (Q), the wormhole size (mm<sup>2</sup>) and microhardness (HV) value. The example calculation is shown below. Meanwhile, all heat generated (Q) values for sample Z1, Z2 and Z3 is shown in Table 4.8 and its relationship with wormhole size and microhardness value is tabulated in Table 4.9. It is also shown graphically in Figure 4.10.

#### Example calculation

For sample Z1, spindle speed = 1,100rpm

$$\begin{aligned} V &= \omega \cdot r = 2 \pi N \cdot r = 2 \pi (1591 \text{ rev/min}) (5 \text{ mm}) \\ &= 50,000 \text{ mm/min} = (50.0 \text{ m/min}) (1 \text{ min}/60 \text{ s}) \\ &= \underline{\underline{0.833 \text{ m/s}}} \end{aligned}$$

$$F = \mu N = (0.5) (1000 \text{ N}) = \underline{\underline{500 \text{ N}}}$$

$$Q = F \cdot v = 0.833 \text{ m/s} \times 500 \text{ N} = \underline{\underline{416.5 \text{ Nm/s}}}$$

**Table 4.8: Result of Heat Generated Calculation**

Sample	Transverse Feed Rate, S (mm/min)	Spindle Speed, N (rpm)	Spindle Speed, N (mm/min)	Ratio (S:N)	Heat Generated, Q (Nm/s)
Z1	50	1,591	50,000	1:1000	416.5
Z2	50	1,353	42,500	1:850	354.2
Z3	50	1,114	35,000	1:700	291.6

**Table 4.9: Relationship of Ratio (S: N), Heat Generated (Q), Wormhole Size (mm<sup>2</sup>) and Microhardness (HV)**

Sample	Ratio (S:N)	Heat Generated, Q (Nm/s)	Wormhole Size (mm <sup>2</sup> )	Microhardness (HV)
Z1	1:1000	416.5	2.58	73.8
Z2	1:850	354.2	2.66	72.4
Z3	1:700	291.6	2.80	70.3

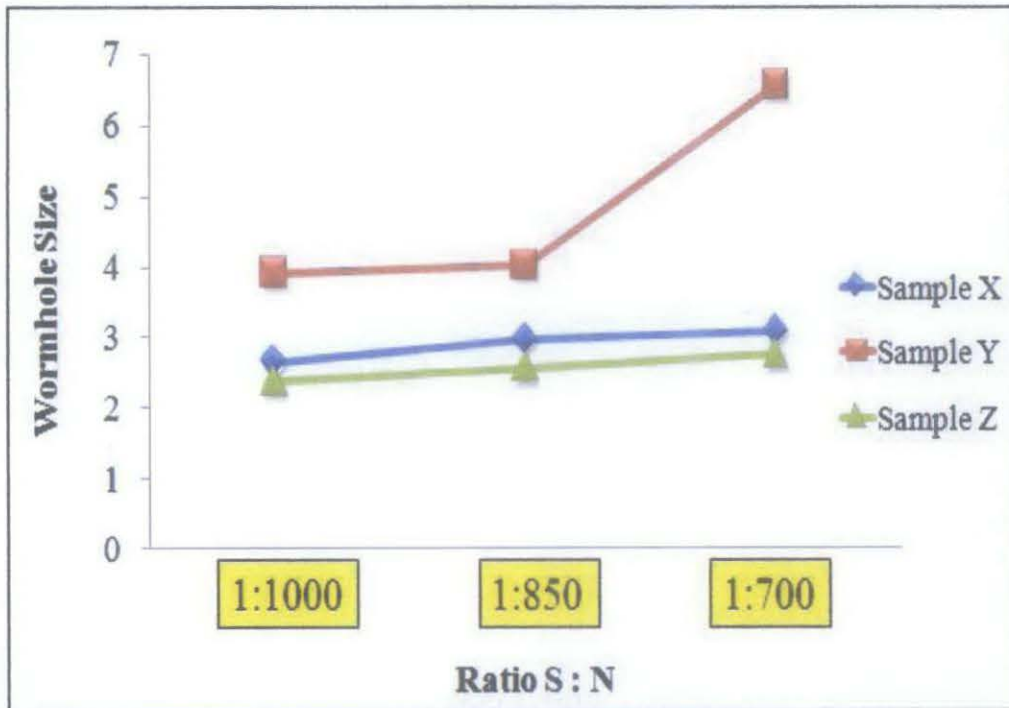


**Figure 4.10: Wormhole Size (mm<sup>2</sup>) vs. Welding Parameter Ratio S: N**

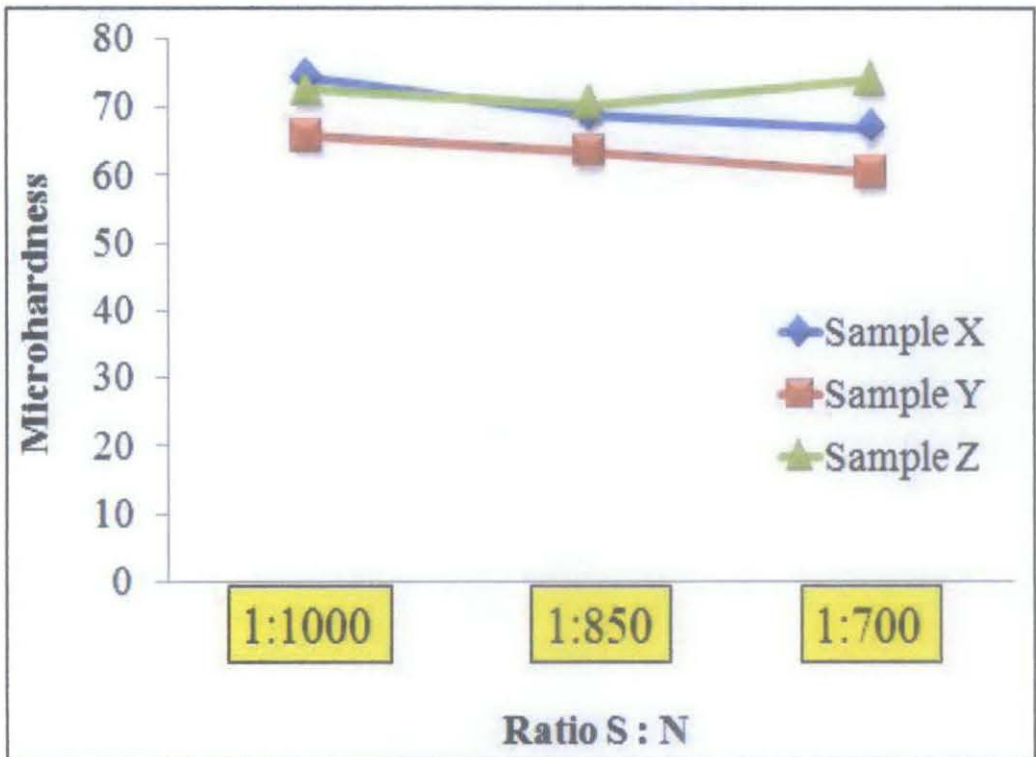


**Figure 4.11: Graph Microhardness (HV) vs. Welding Parameter Ratio S: N**

Based on Figure 4.10 and 4.11, the increase in ratio of transverse feed rate (S) to tool spindle speed (N) from 1: 1000 to 1: 700 will result in increase in the wormhole size (mm<sup>2</sup>) and decrease in Vickers Microhardness (HV). Except for sample Z, due to measurement error, the microhardness values was somehow increase with increasing welding ratio. In order to decrease the wormhole size, it is recommended that ratio S: N should be reduced starting 1:1500, 1:2000 and onwards. Now there lower ratio S: N can be achieve by increasing the spindle speed (rpm) starting from 2000rpm onwards to get more friction and heat generation. At higher heat generated condition, better material flow inside the weld line can be achieved. Furthermore, the transverse speed (mm/min) must be reduced starting from 40mm/min so that the materials have enough time to flow towards the advancing side (AS) and cover back the space that was previously occupied by the tool.

## CHAPTER 5

### CONCLUSIONS AND RECOMMENDATIONS

#### 5.1 Conclusions

Based on the results, several conclusions can be drawn.

1. At a constant welding parameter ratio of transverse feed rate (S) to tool spindle speed (N), increase in spindle speed (rpm) and transverse feed (mm/min) rate favors the initiation of wormhole near the bottom of the weld.
2. At a fixed transverse feed (mm/min), increase in spindle speed (rpm) will result in higher heat generation and decrease in wormhole size.
3. The wormhole size increases from the tool entrance to tool exit. Early observation that the wormhole size is constant throughout a sample has been proven not true.
4. The increase in ratio of transverse feed rate (S) to tool spindle speed (N) will result in increase in the wormhole size (mm<sup>2</sup>) and decrease in Vickers Microhardness value (HV).
5. The lowest microhardness value of a welded plate is at its weld center.
6. Splash occurs because of the material goes out due to the design of welding tool that unable to contain proper material flow. Materials that form splash will result initiation of wormhole defect.

## **5.2 Recommendations**

Here are recommendations for future FSW projects:

1. For future projects, use various method of measuring the wormhole defect size and conclude the most effective method to measure worm defect.
2. FSW process for different series of aluminum alloy can be done.
3. Another Mechanical Testing method which is tensile test can be used to find the relationship with the wormhole initiation.

## REFERENCES

- [1] Kumbhar N.T. and Bhanumurthy K. 2008, *Friction Stir Welding of Al 6061 Alloy*, Asian J. Exp. Sci., Vol 22, No. 2, Trombay, Mumbai.
- [2] Jeffus L. F. 2002, *Welding Principles and Applications, Fifth Edition*, Clifton Park, New York, Delmar Learning.
- [3] Meran. C. 2005, *The Joint Properties of Brass Plates by Friction Stir Welding*, Pamukkale University, Denizli, Turkey.
- [4] Colligan K. 1999, *Material Flow Behavior during Friction Stir Welding of Aluminum*, Welding Research Supplement, 229.
- [5] Mishra R.S. and Mahoney M. W. 2007, *Friction Stir Welding and Processing*, ASM International, Materials Park, Ohio.
- [6] Nandan R., DebRoy T. and Bhadeshia H.K.D.H. 2008, *Recent Advances in Friction Stir Welding – Process, Weldment Structure and Properties*, University of Cambridge, Cambridge.
- [7] Leal R. and A. Loureiro A. 2004, *Defects Formation in Friction Stir Welding of Aluminum Alloys*, Advanced Material Forum II, 302.
- [8] Ahmad Nordin F.A. 2010, *Effect of Welding Tool Geometry on Friction Stir Welding*, Progress Report for Final Year Project, Universiti Teknologi Petronas, Malaysia.
- [9] 'Allauddin M.A. 2009, *an Experimental Study on Microstructure of Friction Stir Welded Plates*, Dissertation Report for Final Year Project, Universiti Teknologi Petronas, Malaysia.
- [10] Classification of Aluminum Alloys,  
[http://www.substech.com/dokuwiki/doku.php?id=classification\\_of\\_aluminum\\_alloys](http://www.substech.com/dokuwiki/doku.php?id=classification_of_aluminum_alloys). (20<sup>th</sup> August 2010)
- [11] Crawford R., Cook G., Strauss A., Hartman D. and Stremmer M. 2006, *Experimental Defect Analysis And Force Prediction Simulation Of High Weld Pitch Friction Stir Welding*. Science and Technology of Welding And Joining, 665.
- [12] Lin H.J., Fujii H., Maeda M. and Nogi K. 2004, *Tensile Fracture Location Characterisation Of The Friction Stir Welded Joints Of Different Aluminium Alloys*, Journal Of Material Science And Technology, 105.

- [13] Long X. and Khanna S.K. 2005, *Modeling Of Electrically Enhanced Friction Stir Welding Process Using Finite Element Method*. Science and Technology of Welding and Joining, 487.
- [14] Zhao Y.H., Lin S.B., Qu F., and Wu L.2006, *Influence of Pin Geometry on Material Flow In Friction Stir Welding Process*, Material Science and Technology.
- [15] Schmidt H. and Hattel J. 2005, *A Local Model For The Thermomechanical Conditions In Friction Stir Welding*. Modelling And Simulation In Material Science And Engineering.
- [16] Elangovan K. and Balasubramaniam V. 2001, *Influences of Pin Profile and Rotational Speed of the Tool on the Formation Of Friction Stir Processing Zone In AA2219 Aluminum Alloy*. Material Science And Technology.
- [17] Kimapong K. and Watanabe T. 2006, *Effect of Welding Process Parameter on Mechanical Properties of FSW Lap Joint between Aluminum Alloy and Steel*. Material Transactions, 2211.
- [18] Reynolds A.P., *Defect Formation in Friction Stir Welds*, The University of South Carolina, United States.
- [19] Valavanis I. and Kosmopoulos D., 2010, *Multiclass Defect Detection and Classification in Weld Radiographic Images Using Geometric And Texture Features*, National Center for Scientific Research Demokritos, Greece.
- [20] Leal R.M., Leitão C., Loureiro A., Rodrigues D.M. and Vilac P., 2008, *Material Flow in Heterogeneous Friction Stir Welding Of Thin Aluminium Sheets: Effect of Shoulder Geometry*, University of Coimbra, Portugal.
- [21] Kumar K. and Kailas S.V., 2007, *The Role of Friction Stir Welding Tool On Material Flow and Weld Formation*. Department of Mechanical Engineering, Indian Institute of Science.
- [22] Haver W. V., Stassart X., deMeester B. and Dhooge A., 2007, *Friction Stir Welding of Aluminium High Pressure Die Castings: Parameter Optimisation and Gap Bidgeability*. Research Center of Belgian Welding Institute (BWI), Universite Catholique de Louvain, & Faculty of Engineering, Ghent University, Belgium.
- [23] Bloodworth T., 2009, *On the Immersed Friction Stir Welding of AA6061-T6: A Metallurgic and Mechanical Comparison to Friction Stir Welding*. Graduate School of Vanderbilt University, Tennessee, United States.

- [24] All Metal Forge Group (Tool Steel),  
<http://www.steelforge.com/ferrous/toolsteel.htm>  
 (22<sup>nd</sup> September 2010)
- [25] Huyett G.L., 2004, *Engineering Handbook*.
- [26] AISI Tool Steel Grade,  
<http://www.wisetool.com/designation/toolsteel.htm#grade>  
 (20<sup>th</sup> August 2010).
- [27] Kalpakjian S. and Schmid S., 2006, *Manufacturing Engineering & Technology 5<sup>th</sup> Edition in SI Units*, 80.
- [28] Cerri E. and Evangelista E., 1999, *Metallography of Aluminium Alloys*.  
 Dipartimento di Meccanica, Università di Ancona, Italy.
- [29] BUEHLER® SimpliMet® 1000 & 3000 Automatic Mounting Press –Produce Brochure- pdf (9<sup>th</sup> June 2011)
- [30] Shen Y.L a\*. and Chawla N. b, 2000, *On the Correlation between Hardness and Tensile Strength in Particle Reinforced Metal Matrix Composites*,  
 a. Department of Mechanical Engineering, The University of New Mexico, Albuquerque, USA.  
 b. Mechanical Behavior of Materials Laboratory, Department of Chemical and Materials Engineering, Arizona State University, USA.
- [31] Vickers Microhardness Testing,  
<http://www.hardnesstesters.com/Applications/Vickers-Hardness-Testing.aspx>  
 (27<sup>th</sup> July 2011)
- [32] Principles of Field Emission Scanning Electron Microscope (FESEM),  
<http://infohost.nmt.edu/~mtls/instruments/Fesem/FESEM%20principle.htm>  
 (2<sup>nd</sup> June 2011)
- [33] Aluminum Alloy 6061 Series,  
[http://www.substech.com/dokuwiki/doku.php?id=wrought\\_aluminum-magnesiumsilicon\\_alloys\\_6xxx&DokuWiki=b802597b7efa9f61cc0138f0d883e1f1](http://www.substech.com/dokuwiki/doku.php?id=wrought_aluminum-magnesiumsilicon_alloys_6xxx&DokuWiki=b802597b7efa9f61cc0138f0d883e1f1) (9<sup>th</sup> June 2011)
- [34] Song M., Kovacevic R., Ouyang J. And Valant M., 2002, *A Detailed Three-Dimensional Transient Heat Transfer Model for Friction Stir Welding*.  
 Department of Mechanical Engineerin, Southern Methodist University, Richardson, Texas, USA.

## APPENDICES

### Final Year Project (FYP) I Gantt Chart.

No	Detail/Week	1	2	3	4	5	6	Mid Semester Break	7	8	9	10	11	12	13	14	
1	Selection of Project Topic	█															
2	Literature review. Concept familiarization of Friction Stir Welding (FSW).	█	█														
3	Literature Review Worm (Tunnel) Defect of Aluminum Alloy Friction Stir Welded Plates.			█	█	█	█			█	█	█	█	█	█	█	█
4	Process of rectifying composition of aluminum alloy plates by X-Ray Fluorescence (XRF) and purchasing Welding Tool Steel H13.									█							
5	Designing of the Welding Tool Steel H13 using AutoCAD 2007.									█							
6	Fabricating the Welding Tool Steel H13 using PowerPath 15 (CNC Lathe Machine).										█						
7	Heat treatment process of welding Tool Steel H13 using CARBOLITE heat treatment furnace.											█					
8	Preparation of sample and start trial run of Friction Stir Welding (FSW) using BridgePort 2216 (CNC Milling Machine).												█	█	█		
9	Study & analyze the result Obtained.														█	█	
10	Submission of Final Report and final presentation.															█	

### Final Year Project (FYP) II Gantt Chart.

No	Detail/Week	1	2	3	4	5	6	7	Mid Semester Break								8	9	10	11	12	13	14
1	Study of literature review continues.																						
2	Completes all nine (9) FSW run.																						
3	Material Characterization of aluminum alloy plates using Field Emission Scanning Electron Microscope (FESEM).																						
4	Sectioning of welded aluminum plates using Linear Hacksaw & Abrasive Cutter.																						
5	Mounting of sectioned welded aluminum alloy plates using BUEHLER Phenolic Powder.																						
6	Grinding of mounted welded aluminum alloy plates using different grades (grit) of Silicon Carbide (SiC) grinding paper.																						
7	Polishing of grinded welded aluminum alloy plates using 3 micron Diamond Paste.																						
8	Etching of polished welded aluminum alloy plates using Keller's Reagent.																						
9	Measure the wormhole defect size (area) using Optical Microscope and capture overall image of wormhole using Non Contact Measurement machine.																						
10	Measure hardness value of samples (Vicker -HV) using Microhardness Testing Machine.																						
11	Analyze the result and make conclusion and recommendations for future projects.																						
12	Submission of Final Report and final presentation.																						